PHASE DIAGRAM OF V_2O_5–MoO_3–Ag_2O SYSTEM
Part III. Vanadium-rich part of the diagram

E. Wenda[1]* *and A. Bielański*[1,2]

[1]Faculty of Chemistry, Jagiellonian University, ul. R. Ingardena 3, 30-060 Cracow, Poland
[2]Polish Academy of Sciences, Institute of Catalysis and Surface Chemistry, ul. Niezapominajek 8, 30-239 Cracow, Poland

The results concerning the synthesis, structure and thermal properties of V_2O_5–MoO_3–Ag_2O samples in the vanadium rich region of ternary system are presented in the form of quasi-binary phase diagrams in which at constant V_2O_5/MoO_3 molar ratios, equal 9:1, 7:3 and 1:1, the content of Ag_2O was variable. A new ternary phase isostructural with $NaVMoO_6$ has been detected in the investigated system.

Introduction

Oxide systems containing vanadium and molybdenum play an important role as the catalysts for different oxidation processes first of all oxidation of aromatic and alkyl aromatic hydrocarbons [1, 2]. They are frequently doped with other oxides such as the oxides of cobalt, iron, chromium, phosphorus, sodium, etc. Silver oxide has been shown to enhance selectivity of benzene oxidation to maleic anhydride if added in small amount (of the order of 1 mass%) [3, 4] to the solid solution of MoO_3 in V_2O_5. On the other hand, catalyst may become not active or only weakly active at larger concentrations of silver when vanadium–molybdenum β-bronze and $V_9Mo_6O_{40}$ compound are present as the predominant phases. This is why the knowledge of the physicochemical properties of the V_2O_5–MoO_3–Ag_2O system and in particular the knowledge of its phase diagram is interesting from the point of view of catalysis.

Until now only the binary systems V_2O_5–MoO_3, V_2O_5–Ag_2O and MoO_3–Ag_2O were described in the literature. The V_2O_5–MoO_3 phase diagram has been published by Strupler and Morette [5] and Bielański *et al.* [6]. The work concerning the particular phases appearing in this system has been reviewed in [7]. There is a vast region of solid solubility of MoO_3 in V_2O_5 reaching approximately 30 mol% at eutectic temperature 611°C (this latter temperature has been corrected as 636°C in the present research carried out with more precise method) but it decreases below 500°C in the case of samples containing 10–15 mol% MoO_3 [8].

Doping V_2O_5 with MoO_3 results in the formation of an appropriate number of V^{4+} ions according to the equation:

$$2MoO_3+2V_V \Leftrightarrow 2Mo_V^{\bullet}+5O_0+2V_V^{'}+0.5O_{2(g)} \quad (1)$$
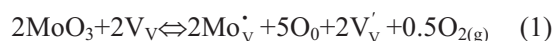
where Kröger–Vink symbols are used. $Mo_V^{\bullet}$ represents Mo atom in the oxidation state VI in the cationic position, O_0 oxygen atom in the oxidation state –II in the anionic position and $V_V^{'}$ an excess electron localized on V^{5+} i.e. vanadium atom in the oxidation state IV.

An intermediate compound $V_9Mo_6O_{40}$ congruently fusing at about 660°C appears in the V_2O_5–MoO_3 system. Depending on calcination temperature the composition of $V_9Mo_6O_{40}$ phase may vary within certain limits [9, 10] and this is why some earlier authors proposed V_2MoO_8 formula. The solid solution of MoO_3 in V_2O_5 phase and $V_9Mo_6O_{40}$ phase are forming an eutectic melting at about 636°C, to which composition about 45 mol% of MoO_3 corresponds. The part of the phase diagram corresponding to the higher MoO_3 content than in $V_9Mo_6O_{40}$ represents a typical two-component phase diagram without the formation of solid solution of V_2O_5 in the usual orthorhombic modification of MoO_3. The eutectic containing about 60 mol% MoO_3 melts at 645°C.

The MoO_3–Ag_2O system has been investigated by Kohmüller and Fourie [11] and one of the present authors [12]. In the former case the range of 0–50 mol% Ag_2O was studied and the range of 0–100 mol% Ag_2O in the latter one. There are two congruently melting compounds appearing in this system: $Ag_2Mo_4O_{13}$ (536°C) and $Ag_2Mo_2O_7$ (516°C) as well as one incongruently melting β-Ag_2MoO_4 (575°C). They are forming three eutectic subsystems. All the above compounds are stoichiometric and contain molybdenum in its highest oxidation state (VI). However β-Ag_2MoO_4 melts incongruently decomposing at 575° according to the equation:

*   Author for correspondence: wenda@chemia.uj.edu.pl

$$\beta\text{-Ag}_2\text{MoO}_4 \Leftrightarrow \text{Ag} + \text{liquid} \qquad (2)$$
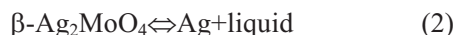
The V_2O_5–Ag_2O system presented in [13] is the most complicated one. Its knowledge is essential for the understanding of the vanadium rich section of the ternary system the object of the present publication. That is why it is shown in Fig. 1. It differs slightly from that in [13] in which the composition limits of β-bronze $Ag_xV_{2-x}O_{5-z}$ below temperature of congruent melting 714°C were not taken into account. Five different phases appear in this system. Two of them: V_2O_5–Ag_2O solid solution and vanadium–silver oxide bronze are non-stoichiometric. The range, within which the value of x in $Ag_xV_{2-x}O_{5-z}$ may change, becomes narrower with the increasing temperature and equals to zero at the composition corresponding to the highest point of the liquidus curve. The formation of vanadium–silver oxide bronze is due to reaction:

$$\text{Ag}_2\text{O} + 2V_V \Leftrightarrow 2\text{Ag}_i^{\cdot} + 2V_V^{'} + 0.5\text{O}_2 \qquad (3)$$
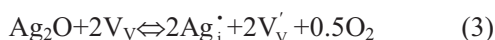
where vanadium is partly reduced to the oxidation state IV. Maximal concentration of V^{4+} has been found at the composition 14.8 mol% Ag_2O. The same sample exhibits the highest temperature of fusion 714°C (point C). Its composition corresponds to the formula: $Ag_{0.3}V_{1.7}O_{4.25}$. On cooling the β-bronze enters at 550°C into meritectic reaction:

$$\beta\text{-bronze} + \text{liquid} \Leftrightarrow \text{Ag}_2\text{V}_4\text{O}_{11} \qquad (4)$$

The $Ag_2V_4O_{11}$ compound is incongruent and on further cooling the sample another meritectic reaction occurs at 470°C:

$$\text{Ag}_2\text{V}_4\text{O}_{11} + \text{liquid} \Leftrightarrow \beta\text{-AgVO}_3 \qquad (5)$$
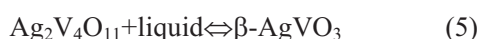
As Fig. 1 shows eutectic β-$AgVO_3$–Ag_3VO_4 corresponds to the composition of 62.5 mol% Ag_2O and solidifies at 376°C (point F). Silver vanadate Ag_3VO_4 is fusing incongruently and decomposes with the segregation of metallic silver at 450°C:

$$\text{Ag}_3\text{VO}_4 \Leftrightarrow \text{Ag} + \text{liquid} \qquad (6)$$

Despite the fact that the three binary systems V_2O_5–MoO_3, V_2O_5–Ag_2O and MoO_3–Ag_2O are known no any investigation of the triple system V_2O_5–MoO_3–Ag_2O was undertaken in the literature and hence the aim of the present research was to gather the basic information concerning this system. The study does not comprise the silver oxide reach region of the triple system where, as already was said, the formation of metallic silver takes place as it is shown by the Eqs (2) and (6).

The present paper is the continuation of the earlier papers published by one of the present authors as Part I [13] describing V_2O_5–Ag_2O system and Part II [12] concerning the MoO_3–Ag_2O system and deals with the vanadium reach region of the triple system

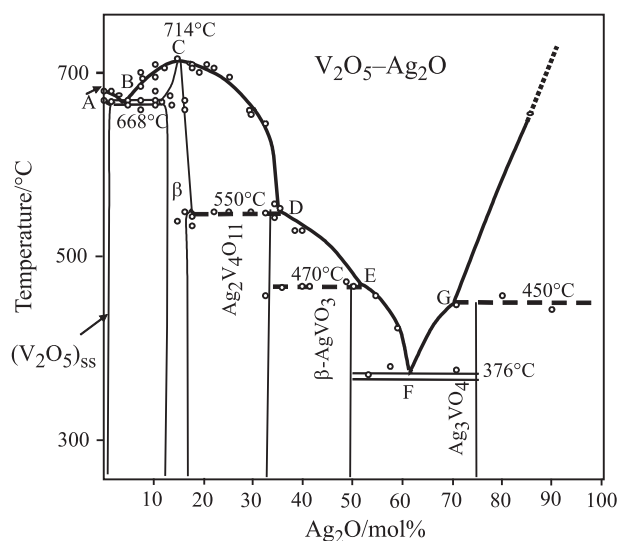**Fig. 1** Phase diagram of V_2O_5–Ag_2O system (according to [13])

V_2O_5–MoO_3–Ag_2O. In the following papers we intend to present the molybdenum reach part of the system and subsequently to discuss the phase diagram of V_2O_5–MoO_3–Ag_2O system.

Experimental

V_2O_5–MoO_3–Ag_2O samples were obtained by mixing at first V_2O_5 (p.a. 'Analar') and MoO_3 (p.a. 'Reanal') in following fixed ratios:

1)   90 mol% V_2O_5 – 10 mol% MoO_3

2)   70 mol% V_2O_5 – 30 mol% MoO_3

3)   50 mol% V_2O_5 – 50 mol% MoO_3

Subsequently appropriate amounts of Ag_2O (p.a. POCH Gliwice) were added thus giving a series of samples with fixed V_2O_5/MoO_3 ratio and variable content of Ag_2O. The mixtures were homogenised for 24 h in pebble mill. On still longer homogenisation time the formation of small amounts of metallic silver was observed. Samples were heated in the atmosphere of air at temperatures about 50°C below the melting point. The information concerning the melting temperatures of all samples presented in this work was obtained from the preliminary thermal analysis of the initial oxide mixtures. At temperatures as high as 600–650°C the reactions were fast enough and no pressing was necessary. On the other hand the samples heated at 360–500°C had to be pressed into pellets. In the first series of experiments (Table 1) the samples were heated with different rates up to a fixed temperature and immediately cooled down in the furnace according to the accepted program. In the second series of the experiments the samples after reaching a certain temperature were kept at it for a certain period

of time and cooled down at two different rates (Table 2). In the third series of the experiments the conditions of the samples preparation varied dependently on the silver oxide concentration (Table 3). In particular the samples containing 25–90 mol% Ag_2O were pelleted and heated for 24 or more hours at the temperatures given in the table. Subsequently the pellets were crushed, analysed and examined by XRD. The samples were then pelleted and again heated at appropriate sintering temperature. This procedure was repeated until no changes in XRD pattern or DTA curve were observed. The method of heating and cooling the samples was essentially the same as it was applied in a number of papers concerning metal oxide system, e.g. [18–35]. The information concerning the synthesis of particular samples is given in Tables 1–3.

DTA and DTG analyses were carried out using Mettler and also SDT 2960 TA Instruments thermoanalysers. The position of DTA peak could be read using our instruments with the precision of the order of 1k and 0.1K, respectively. In most cases heating rate

$10°C\ min^{-1}$ was applied. Temperatures of endothermic effects (no exothermic ones were observed) have been used to determine the points on liquidus and solidus lines corresponding to the particular set of the samples.

The X-ray powder diagrams of samples were obtained using X-ray Seifert spectrometer and CuK_α radiation. Phase identification was carried out by comparing the obtained data with ASTM and ICDD-PDF using computer program or with the data in original papers [14, 15]. The results are given in Tables 1–3.

Results and discussion

Phase diagram sections presented in this paper were constructed basing on DTA analysis supported by the results of X-ray phase analysis. There are two procedures in the interpretation of DTA effects. The first of them which may be called the onset method determines the very beginning of the observed effect. The characteristic onset temperature corresponds in DTA

Table 1 Samples with V_2O_5/MoO_3 molar ratio 9:1[x]. Sintering conditions, phase composition and DTA analysis

Ag_2O/ mol%	Heating rate/ $°C\ h^{-1}$	Sintering T/$°C$	Average cooling rate/$°C\ h^{-1}$	Phase composition	T of DTA endothermic effects/$°C$	Remarks
1	4.4	630	72	$(V_2O_5)_{ss}$, β-bronze $V_9Mo_6O_{40}$	677	sample non pelleted
2	6.6	630	72	as above	674	as above
3	6.5	620	48	as above	671	as above
4	8.6	620	72	as above	669	as above
5	6.5	620	48	as above	666, 688	as above
7.5	4.3	620	48	as above	666, 700	as above
10	5.3	640	48	as above	672, 708	as above
12.5	4.5	650	72	as above	575, 672, 714	as above
15	4.0	680	264	β-bronze, $(V_2O_5)_{ss}$-traces	556, 669, 724	as above
17.5	6.5	620	72	β-bronze, $AgVMoO_6$	550, 642, 708	as above
20	6.5	620	72	β-bronze, $Ag_2V_4O_{11}$ $AgVMoO_6$ (traces)	560, 716	sample kept at sintering T for 10 h
30	7.6	550	6	as above	564, 664	pellet sample kept at sintering T for 10 h
40	4.2	500	24	β-$AgVO_3$, $Ag_2V_4O_{11}$, $AgVMoO_6$	483, (527), 550	pellet
50	7.3	350	cooling with furnace	β-$AgVO_3$, β-Ag_2MoO_4	360, 480	as above
60	7.3	350	as above	β-$AgVO_3$, β-Ag_2MoO_4 Ag_3VO_4	370, 405	as above
70	7.3	350	as above	Ag_3VO_4, β-Ag_2MoO_4 β-$AgVO_3$	375, 455	as above
80	7.3	350	as above	Ag_3VO_4, Ag	450, 635	as above

[x]samples cooled down after reaching 'sintering temperature'

Table 2 Samples with V_2O_5 /MoO_3 molar ratio 7:3. Sintering conditions, phase composition and DTA analysis

Ag_2O/ mol%	Heating rate/ °C h^{-1}	Sintering T/°C	Time of sintering/h	Average cooling rate/°C h^{-1}	Phase composition	T of DTA endothermic effects/°C	Remarks
1	264	660	24	260	$(V_2O_5)_{ss}$, β-bronze, $V_9Mo_6O_{40}$	555, 635, 655	sample non pelleted
2	264	660	24	260	as above	560, 620, 650	as above
3	264	600	24	86	as above	622, 644	as above
5	264	660	24	260	as above	620, 638, 665	as above
7.5	264	560	24	86	as above	613, 643, 684	as above
10	264	660	24	86	as above	585, 630, 700	as above
12.5	264	560	24	85	as above	588, 635, 692	as above
15	264	600	24	85	β-bronze, $V_9Mo_6O_{40}$, $AgVMoO_6$	600, 708	as above
17.5	24.2	510	24	88	as above	600, 685	as above
20	264	660	24	86	β-bronze, $AgVMoO_6$, $Ag_2V_4O_{11}$	553, 607, 700	as above
22.5	264	580	48	86	as above	550, 592, 690	as above
25	264	580	48	86	as above	555, 591, 667	as above
30	264	560	48	85	$AgVMoO_6$, $Ag_2V_4O_{11}$	550, 560, 620	as above
40	10.4	420	48	86	$Ag_2V_4O_{11}$, β-$AgVO_3$, $AgVMoO_6$	482, 544	as above
50	250	350	48	86	β-$AgVO_3$, β-Ag_2MoO_4	365, 430, 500	pellet
60	250	340	48	85	β-$AgVO_3$, β-Ag_2MoO_4	370	as above
70	275	320	48	86	β-$AgVO_3$, β-Ag_2MoO_4, Ag_3VO_4	370, 450	as above
80	250	400	48	86	β-Ag_2MoO_4 (traces), Ag_3VO_4, Ag	325, 450, 520	as above

diagram to the intersection of the extrapolated base-line and the tangent through the inflection point on the leading edge of the peak [17]. The other method characterising the DTA effects consists in determining the temperature corresponding to maximum of the DTA peak. Physically it is the temperature read at the moment when the heat consumption rate is most rapid. In our investigation in same cases – mostly when overlapping of the effects occurred – the course of base-line could not be determined univocally and hence we decided to apply the second method for all the samples. The difference between the onset and peak temperatures was tested by us on the case of 21 different samples of V_2O_5–MoO_3–Ag_2O system on which the onset method could be univocally applied. The average value of ΔT was 11.5±4.6° which characterises the difference between both methods in case of our metal–oxide system.

In determination of liquidus and solidus lines in binary system several interpretations of DTA peaks are possible. A single symmetric narrow DTA peak was ascribed to the congruently fusing compound or to an eutectic. A broad asymmetric peak indicates the pres-

ence of a mixture of phases of the average composition close to that of congruent compound or eutectic. Most frequently two DTA peaks were observed. Peak at lower temperature corresponds to the fusion of eutectic and the other one – to the fusion of the component of the binary system present in an excess as compared with the eutectic composition. Two peaks are present also when compound with incongruent melting point is present in the binary system. The case in which three endothermic DTA peaks were registered was interpreted as the presence of two compounds with incongruently melting points. In the ternary system the situation is much more complicated. We can observe here endothermic effects on one sample: corresponding to the fusion of ternary eutectic, the fusion of binary eutecic along eutectic line and the fusion of single compound phase. However, in many cases we observe two or even only one broad asymmetric DTA peak if the investigated sample exhibits the composition similar to that of double eutectic or one of the triple points. An additional difficulty in the studied ternary system is connected with the non stoichiometric bronze phase which at each point of the Gibbs diagram exhibits dif-

Table 3 Samples with V_2O_5/MoO_3 molar ratio 1:1. Sintering conditions, phase composition and DTA analysis

| $Ag_2O/$ mol%	Heating rate/ °C h^{-1}	Sintering T/°C	Time of sintering/h	Average cooling rate/°C h^{-1}	Phase composition	T of DTA endothermic effects/°C	Remarks
1	256	660	24	128	$V_9Mo_6O_{40}$, $(V_2O_5)_{ss}$, β-bronze	560, 630, 650	sample non pelleted
2	256	660	24	128	$V_9Mo_6O_{40}$, $(V_2O_5)_{ss}$, β-bronze	570, 610, 620	as above
5	256	660	24	128	$V_9Mo_6O_{40}$, β-bronze	563, 650	as above
10	256	660	24	128	$V_9Mo_6O_{40}$, β-bronze	590, 670	as above
15	256	660	24	128	$AgVMoO_6$, $V_9Mo_6O_{40}$, β-bronze	540, 590	as above
20	256	660	24	128	$AgVMoO_6$, β-bronze, $V_9Mo_6O_{40}$ (tr)	610	as above
25	2.2	520	168	86	$AgVMoO_6$, β-bronze, $Ag_2V_4O_{11}$	550, 605	pellet
30	2.6	470	96	86	$AgVMoO_6$, $Ag_2V_4O_{11}$	555, 600	as above
35	2.4	420	72	86	$AgVMoO_6$, β-$AgVO_3$, β-Ag_2MoO_4	459, 545	as above
40	2.3	450	96	86	$AgVMoO_6$, β-$AgVO_3$, β-Ag_2MoO_4	475, 540	pellet
45	300	320	48	86	$AgVMoO_6$, β-$AgVO_3$, β-Ag_2MoO_4	434, 466	as above
50	2.3	450	96	86	β-Ag_2MoO_4, β-$AgVO_3$	360, 430, 450	as above
55	300	320	48	86	β-Ag_2MoO_4, β-$AgVO_3$, Ag_3VO_4	370, 405	as above
60	300	320	72	86	β-Ag_2MoO_4, β-$AgVO_3$, Ag_3VO_4	370	as above
70	300	320	24	86	β-Ag_2MoO_4, Ag_3VO_4, Ag	375, 455, 500	as above
80	1.8	400	96	86	as above	365, 448, 490	as above
90	1.8	400	96	86	as above	459, 520, 540	as above

ferent composition and different characteristic temperatures. The interpretation of the results obtained for ternary system has to be done by comparing simultaneously the results of DTA, X-ray phase analysis and apply the general rules of projecting liquidus planes on the plane of Gibbs triangle.

Figures 2–4 show the cross sections of the V_2O_5–MoO_3–Ag_2O ternary system in which at constant V_2O_5/MoO_3 molar ratio (equal to 9:1, 7:3 and 1:1) the content of Ag_2O was variable. In each of them the temperatures of DTA effects corresponding to the particular samples are given. The temperature of the highest DTA peak was assumed as the melting point of the sample determining the course of liquids represented by full thick line. The DTA peaks at lower temperatures correspond to different thermic effects: melting of the binary or ternary eutectics or the meritectic reactions. Particular diagrams are described in the following section of the present paper. However it should be observed that the results of the present investigation will be used for the construction of the full three dimensional ternary diagram in the last paper of the presented series. Then the more ample discussion of crystallisation processes in V_2O_5–MoO_3–Ag_2O system will be given.

Besides the phases present in the binary systems: V_2O_5–MoO_3, V_2O_5–Ag_2O and MoO_3–Ag_2O mentioned in the Introduction the following ternary phases containing all three components were observed in the V_2O_5 reach part of diagram:
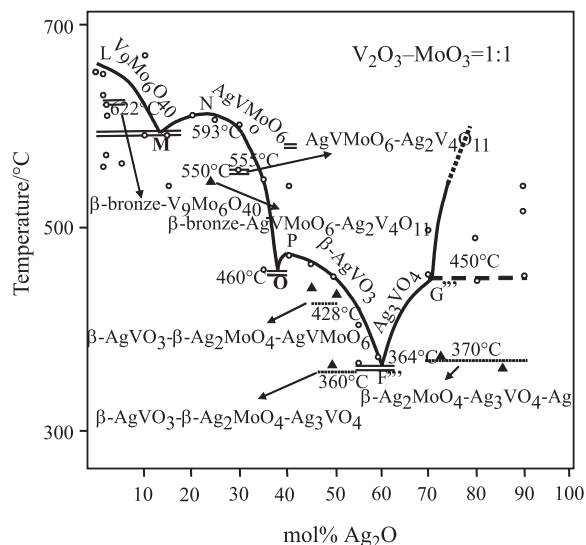
- Solid solution of Ag_2O and MoO_3 in V_2O_5, $(V_2O_5)_{ss}$, exhibits the structure of V_2O_5 in which lattice parameters are somewhat larger than in the case of undoped V_2O_5. The incorporation of MoO_3 is assumed to occur according to Eq. (1) and that of Ag_2O according to Eq. (3). This ternary phase is stable within low content of Ag_2O, not higher than 1 mol%.
- Solid solution of MoO_3 in vanadium–silver–oxide β-bronze $Ag_xMo_yV_{2-(x+y)}O_{5-z}$ (described in Introduction); Mo^{6+} ions substitute V^{5+} ions (Eq. (1)) in octahedra and Ag^+ ions are situated in the channels present in the structure. At x=0.30 (15 mol% Ag_2O) it reaches maximal temperature of fusion: 724°C
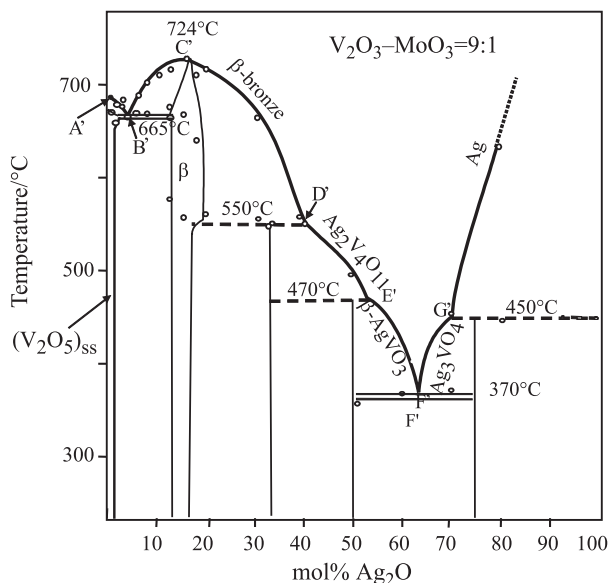
Fig. 2 $V_2O_5:MoO_3=9:1$ section of the ternary $V_2O_5–MoO_3–Ag_2O$ diagram. Thick full lines represent the cross-section of the (9:1) diagram plane with crystallisation fields in the ternary system. Points on == represent the cross section of double eutectic lines in ternary system with the (9:1) diagram plane. Points on – – represent the cross-section of the boundary planes along which meritectic reaction occurs in the ternary system with the (9:1) diagram plane

Fig. 4 $V_2O_5:MoO_3=1:1$ section of the ternary $V_2O_5–MoO_3–Ag_2O$ diagram. Thick full lines represent the cross section of the (1:1) diagram plane with crystallisation fields in the ternary system. Points on == represent the cross section of double eutectic lines in ternary system with the (1:1) diagram plane. Points on --- represent the cross-section of the boundary planes along which meritectic reaction occurs in the ternary system with the (1:1) diagram plane. ▲ – temperature of ternary eutectic temperature points
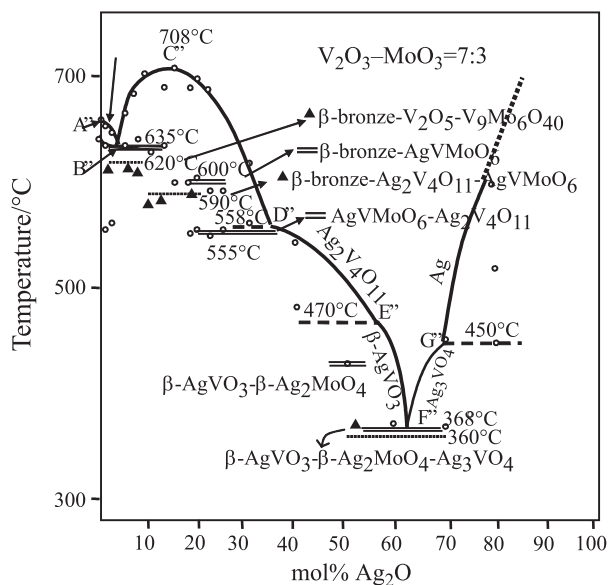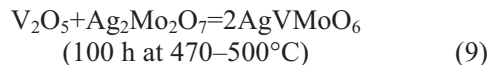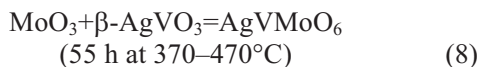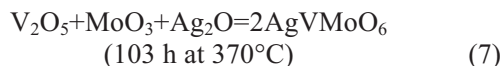

Fig. 3 $V_2O_5:MoO_3=7:3$ section of the ternary $V_2O_5–MoO_3–Ag_2O$ diagram. Thick full lines represent the cross section of the (7:3) diagram plane with crystallisation fields in the ternary system. Points on == represent the cross section of double eutectic lines in ternary system with the (7:3) diagram plane. Points on – – represent the cross-section of the boundary planes along which meritectic reaction occurs in the ternary system with the (7:3) diagram plane. ▲ – temperature of ternary eutectic fusion points

occurring without change of composition. This indicates that there exists maximum in the field of β-bronze crystallisation in the ternary phase diagram. The bronze reaches at this point composition corresponding to an approximate formula: $Ag_{0.30}Mo_{0.08}V_{1.54}^{5+}V_{0.08}^{4+}O_{4.44}$. The approximate range of the β-bronze composition at which the melt solidifies as one phase only is marked by β on the diagram in Fig. 2. Interplanar distances obtained in XRD studies of bronzes investigated in [14, 15] as well as in this study are presented in Table 4. The values obtained for $Ag_{0.35}V_2O_5$ [14] are given in column 1 (experimental data). The values obtained for $Li_{0.30}V_{1.70}Mo_{0.30}O_5$ [15] as well as for $Ag_{0.30}Mo_{0.08}V_{1.54}^{5+}V_{0.08}^{4+}O_{4.40}$ (this study) are given in columns 2 and 3, respectively. The fact that all these distances are very much similar suggests that β-bronze structure does not depend (to some extent) on the content of molybdenum and rather weakly depends on the kind of monovalent ions present in the channels of the crystal lattice.

- The samples of the composition close to $AgVMoO_6$ exhibit X-ray pattern practically identical with that of $NaVMoO_6$ [Table 5 column 1]. They are fusing at a constant temperature 625°C. This phase has been obtained by heating in air, at appropriate temperatures, the mixtures of the following compounds pressed into the pellets:

$$V_2O_5 + MoO_3 + Ag_2O = 2AgVMoO_6$$
$$(103 \text{ h at } 370°C) \quad (7)$$

$$MoO_3 + \beta\text{-}AgVO_3 = AgVMoO_6$$
$$(55 \text{ h at } 370–470°C) \quad (8)$$

$$V_2O_5 + Ag_2Mo_2O_7 = 2AgVMoO_6$$
$$(100 \text{ h at } 470–500°C) \quad (9)$$

Each of the above reactions led to the product exhibiting practically the same X-ray diagram (Table 5). The DTA curve of the sample obtained according to Eqs (7–9) is shown in Fig. 5.

V$_2$O$_5$:MoO$_3$=9:1 section of the ternary diagram is shown in Fig. 2. In accordance with the fact that there was a high excess of vanadium over molybdenum this diagram is very much similar to that of V$_2$O$_5$–Ag$_2$O system and the same phases are present. The compounds of molybdenum V$_9$Mo$_6$O$_{40}$, β-Ag$_2$MoO$_4$ and AgVMoO$_6$ phase (isostructural with NaVMoO$_6$), the crystallisation fields of which are situated in molybdenum reach region of the ternary diagram, are present in definitely small amounts. Their properties and role in crystallisation will be discussed in a later paper.
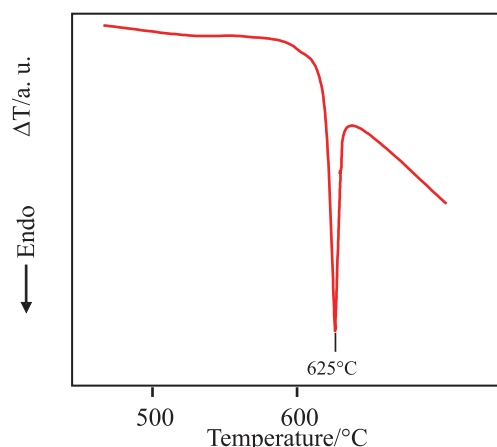
Table 4 X-ray diffraction lines of isostructural β-bronzes

Ag$_{0.35}$V$_2$O$_5$ [14]		Li$_{0.30}$V$_{1.70}$Mo$_{0.30}$O$_5$ [15]		Ag$_{0.30}$Mo$_{0.08}$V$_{1.62}$O$_{4.40}$ [this work]	
1		2		3	
d/nm	I/I_0	d/nm	I/I_0	d/nm	I/I_0
		0.9650	90	0.957	70
0.720	12	0.7270	100	0.7224	2
0.696	8	0.6910	16	0.7089	10
–	–	0.5110	6	–	–
0.472	40	0.4820	25	0.4751	100
0.383	40	0.3810	6	0.3842	6
–	–	0.3640	16	–	–
0.350	12	0.3560	20	0.3514	10
0.337	20	0.3400	20	0.3386	3
–	–	0.3250	6	0.3212	6
–	–	0.3220	20	0.3163	25
0.305	100	0.3110	60	0.3063	30
0.2910	55	–	–	0.2917	10
0.2887	50	0.2886	40	0.2889	4
0.2720	40	0.2728	10	0.2729	4
0.2616	5	–	–	0.2629	10
–	–	0.2532	16	0.2554	7
0.2443	12	0.2475	6	0.2454	4
0.2363	12	–	–	0.2376	77
–	–	0.2412	16	–	–
–	–	0.2372	10	–	–
–	–	0.2305	6	–	–
–	–	0.2276	10	–	–
0.2164	18	0.2204	40	0.2175	12
–	–	0.2026	8	0.2048	22
0.1971	25	0.1973	25	0.1976	23
–	–	0.1947	6	–	–
–	–	0.1908	8	–	–
–	–	0.1897	8	–	–
0.1861	12	–	–	0.1868	27
0.1802	30	–	–	–	–
–	–	0.1705	–	0.1709	31

Table 5 X-ray diffraction lines pattern of the samples $AgVMoO_6$ obtained by different methods as compared with $NaVMoO_6$ compound

NaVMoO₆ [16]		AgVMoO₆ Reaction (7)		AgVMoO₆ Reaction (8)		AgVMoO₆ Reaction (9)	
1		2		3		4	
d/nm	I	d/nm	I	d/nm	I	d/nm	I
0.6748	999	0.6838	5	0.679	10	0.6676	19
0.4494	28	0.4563	12	0.4545	7	0.4470	23
0.4398	162						
0.3376	282m	0.3407	62	0.3397	66	0.3369	100
0.3311	198	0.3341	63	0.3331	57	0.3296	68
0.3200	623	0.3253	100	0.3238	87	0.3210	79
0.2865	21	0.2893	26	0.2883	13	0.2860	32
0.2569	80	0.2588	16	0.2580	16	0.2560	26
–		–	–	0.2397	11	–	–
0.2377	147	0.2389	7	0.2381	9	0.2371	33
0.2354	28	–	–	–	–	–	–
0.2303	141	–	–	–	–	0.2314	11
0.2873	15	0.2268	90	0.2264	100	–	–
0.2247	120m	0.2236	7	0.2226	6	0.2249	97
0.2200	3m	0.2217	6	0.2216	6	0.2209	14
0.2003	98m	–	–	–	–	0.2005	17
0.1963	71	0.1976	12	0.1975	8	0.1966	14
0.1899	6	–	–	–	–	–	–
0.1889	2						
0.1828	107	0.1836	12	0.1831	4	0.1820	21
0.1806	55	0.1816	13	0.1816	7	0.1805	12
0.1765	142m	0.1778	26	0.1777	15	0.1767	25

Due to the presence of third component (introduced into V_2O_5–Ag_2O system) the number of the freedom degrees increased by one and the liquidus lines of quasi-binary system shown in Fig. 2 are now lying on the crystallisation fields of ternary diagram and eutectic points of the farmer one are lying on double eutectic lines in the latter. The eutectic point B at 3.5 mol% Ag_2O (Fig. 1) in V_2O_5–Ag_2O system has its analogy in point B′ (Fig. 2) in the ternary system. This latter point is situated on double eutectic line in the ternary system along which crystallisation fields of $(V_2O_5)_{ss}$ and vanadium–molybdenum–silver bronze intersect. These section of the diagram cuts also the crystallisation field of β-bronze (along the B′C′D′ line), $Ag_2V_4O_{11}$ (line D′E′), β-$AgVO_3$ (line E′F′) and Ag_3VO_4 (line F′G′) as well as the lines of the meritectic equilibria:

β-bronze/$Ag_2V_4O_{11}$ (point D′ reaction 4)

$Ag_2V_4O_{11}$/β-$AgVO_3$ (point E′ reaction 5)

Ag_3VO_4/Ag   (point G′ reaction 6)

Fig. 5 DTA curve of $AgVMoO_6$ phase obtained according to Eq. (10)

and also the line of double eutectic at 370°C (F′) dividing β-$AgVO_3$ and Ag_3VO_4 crystallisation fields.

V_2O_5–MoO_3=7:3 section of the ternary diagram is shown in Fig. 3. On this cross-section only liquidus lines, temperature of binary eutectics, temperature and the range of meritectic reactions (4)–(6) as well as tem-

perature of ternary eutectic fusion points are shown. The course of the liquidus line is similar to those presented in Figs 1 and 2. However temperatures, at which double eutectic are fusing are shifted to lower values. The eutectic point B″ situated on the intersection line of crystallisation fields of vanadium oxide phase and β-bronze (boundary curve) is lowered to 635°C as the effect of increased content of MoO_3. The same effect is observed in the case of point F″ situated on the intersection line of the crystallisation fields of β-$AgVO_3$ and Ag_3VO_4, temperature corresponding to it is lowered to 368°C. Also the maximum (point C″) on the crystallisation field of β-bronze is lowered to 708°C. It should be observed that the increased content of molybdenum results in the appearance of the molybdenum rich compounds $V_9Mo_6O_{40}$ and $AgVMoO_6$ (Table 2). The course of the crystallization of the latter one will be discussed in the following papers.

V_2O_5:MoO_3=1:1 section of the ternary diagram is shown in Fig. 4. In this case the crystallisation fields of the $V_9Mo_6O_{40}$ and $AgVMoO_6$ phases are cut along LM and MO lines, respectively. Both compounds are forming double eutectic the line of which is cut by the 1:1 cross section plane at point M (at 12.5 mol% Ag_2O) to which temperature 593°C corresponds. Similarly $AgVMoO_6$ and β-$AgVO_3$ are forming a double eutectic in the ternary system. Its line cuts 1:1 cross section plane at 460°C and 37 mol% Ag_2O (point O). The temperature of the analogous eutectic point of β-$AgVO_3$–Ag_3VO_4 is now lowered to 364°C at 60 mol% Ag_2O.

Conclusions

The paper presents the vanadium rich sections of the ternary V_2O_5–MoO_3–Ag_2O system in which at constant V_2O_5/MoO_3 ratio (equal to 9:1, 7:3 and 1:1) the concentration of Ag_2O was variable. In the investigated system the same phases appeared as those present in the binary V_2O_5–Ag_2O system. The X-ray diffraction pattern indicated also the presence of a new phase isomorphic with $NaVMoO_6$ compound for which tentatively formula $AgVMoO_6$ was proposed.

References

1 L. Ya. Margolis, Okislenie uglevodorov na geterogennikh katalizatorakh. 'Khemia', Moscow 1977, p. 96.
2 A. Bielański and J. Haber, Oxygen in Catalysis, Marcel Dekker, New York 1991,p. 137.
3 A. Bielański, J. Poźniczek and E. Wenda, Bull. Pol. Ac. Sci. Chem., 24 (1976) 415.
4 A. Bielański and J. Poźniczek, React. Kinet. Catal. Lett., 33 (1987) 417.
5 N. Strupler and A. Morette, Compt. Rend. Chim. Miner., 260 (1965) 1971.
6 A. Bielański, K. Dyrek, J. Poźniczek and E. Wenda, Bull. Pol. Ac. Sci. Chem., 19 (1971) 507.
7 A. Bielański and M. Najbar, Appl. Cat. A: General, 157 (1997) 223.
8 A. Bielański and M. Najbar, Pol. J. Chem., 52 (1978) 883.
9 R. H. Jarman, P. G. Dickens and A. J. Jacobson, Mater. Res. Bull., 17 (1982) 325.
10 R. H. Jarman and A. K. Cheetham, Mater. Res. Bull., 17 (1982) 1011.
11 R. Kohmüller and J. P. Fourie, Bull. Soc. Chim. Fr., 11 (1968) 4379.
12 E. Wenda, J. Thermal Anal., 36 (1990) 1417.
13 E. Wenda, J. Thermal Anal., 30 (1985) 879.
14 A. Casalot and P. Pouchard, Bull. Soc. Chim. Fr., 10 (1967) 3817.
15 J. Galy, J. Darriet and D. Canalis, C. R. Acad. Sc. Paris, 264, ser. C(7) (1967) 579.
16 Powder Diffraction File, International Centre for Diffraction Data, File Nos.: 04-002-4831.
17 D. Kobertz, M. Miller, U. Niemann, L. Singheiser and K. Hilpert, Thermochim. Acta, 430 (2005) 73.
18 M. Kurzawa and M. Bosacka, J. Therm. Anal. Cal., 56 (1999) 211.
19 M. Kurzawa and G. Dąbrowska, J. Therm. Anal Cal., 56 (1999) 217.
20 M. Kurzawa and M. Bosacka, J. Therm. Anal. Cal., 65 (2001) 451.
21 J. Walczak, M. Kurzawa and E. Filipek, Thermochim. Acta, 117 (1987) 9.
22 J. Walczak, M. Kurzawa and P. Tabero, Thermochim. Acta, 118 (1987) 1.
23 J. Walczak and E. Filipek, Thermochim. Acta, 150 (1989) 125.
24 J. Walczak and E. Filipek, Thermochim. Acta, 161 (1990) 239.
25 J. Walczak and E. Filipek, Thermochim. Acta, 173 (1990) 235.
26 J. Walczak and E. Filipek, Thermochim. Acta, 228 (1993) 127.
27 J. Walczak and E. Filipek, Thermochim. Acta, 246 (1994) 65.
28 M. Kurzawa and G. Dąbrowska, J. Phase Equilibria, 18 (1997) 147.
29 M. Kurzawa and G. Dąbrowska, Solid State Ionics, 101–103 (1997) 1189.
30 M. Kurzawa, M. Bosacka and P. Jakus, J. Mater. Sci., 38 (2003) 3137.
31 M. Bosacka and M. Kurzawa, Solid State Sci., 7 (2005) 1294.
32 A. Blonska-Tabero and M. Kurzawa, J. Therm. Anal. Cal., 88 (2007) 33.
33 P. Tabero, J. Therm. Anal. Cal., 88 (2007) 37.
34 M. Bosacka, J. Therm. Anal. Cal., 88 (2007) 43.
35 A. Blonska-Tabero, J. Therm. Anal. Cal., 88 (2007) 201.